Numerical modelling of direct currents in 2-D anisotropic structures

Tomáš Verner and Josef Pek
Geophysical Institute, Academy of Sciences of the Czech Republic
Boční II/1401, CZ-14131 Prague 4–Spořilov, Czech Republic

Abstract

Well-known Dey & Morrison's [1] finite difference (FD) algorithm for the 2-D modelling of direct currents is modified for generally anisotropic 2-D structures. By Fourier transforming the general current conservation equation with respect to the strike coordinate, the original $2\frac{1}{2}$-D problem for the potential of a single feeding electrode is decomposed into an infinite number of 2-D problems in the wave number domain. Applying the area discretization (volume integration) scheme to the transformed 2-D PDEs, a 9-point FD stencil is obtained at each mesh node within the anisotropic structure, with generally complex elements for the direct neighbours of the central node. The resulting FD matrix is banded, 9-diagonal, complex and non-symmetric, but Hermitian. Gaussian elimination for real, symmetric and banded matrices is slightly modified to apply to the Hermitian matrices, and used to solve for the wave number potential components. Numerical tests and modelling examples of 2-D anisotropic structures are presented. Extension of the technique to 3-D models with anisotropy is discussed.

1 Introduction

Recently, increased attention has been paid to studies on various aspects of the electrical anisotropy in the earth, motivated in particular by new refined interpretations of deep crustal geoelectrical measurements. Results of several recent regional electromagnetic induction studies, and particularly those accumulated within the KTB project, have considerablely contributed to the recognition of the electrical macro-anisotropy as a real and significant factor of the earth's structure on the crustal scale.

While the large-scale and large-magnitude electrical anisotropy within the deeper earth has been accepted only relatively slowly, the situation in shallow geoelectrical studies is quite different. In the applied geoelectricity, anisotropic rock formations are well known and well documented in many geological environments. The structure and texture of, in particular, the sedimentary and metamorphic rocks often displays directionally non-homogeneous patterns, which, in turn, result in the effective anisotropy of the bulk. Typical anisotropies of common sediments, measured by the anisotropy ratio $\lambda = \sqrt{(\varrho_{\max}/\varrho_{\min})}$, does usually not exceed 2. There are, however, exceptional cases of rocks with extremly high anisotropies. E.g., Karous [2] reports a case of alternating horizons of quartzites and graphitic phyllites from the locality Zlaté Hory in the Ash Mountains (Jeseníky), Moravia, with λ greater than 5.

Numerical simulations are known to be an efficient tool both for analyzing various hypothetic structural settings and for interpreting practical data. For magnetotelluric studies, two general numerical modelling algorithms for anisotropic structures have been published lately, for 2-D [3] as well as for 3-D models [4]. To the best of our knowledge, no analogous simulation technique has been as yet presented for the numerical modelling of direct currents in laterally inhomogeneous anisotropic media. It is the ambition of this paper to fill in this gap, at least for the 2-D structural settings at the moment.

The structure of the paper is as follows: In Section 2, we summarize the governing equations for the propagation of direct currents in generally inhomogeneous media, and formulate the mathematical model for the specific problem of the potential distribution in 2-D anisotropic structures. Section 3 deals with various aspects of the FD approximation of this problem, and with its numerical solution. Section 4 presents simple tests of the algorithm developed, and Section 5 shows an example of the numerical modelling for a simple synthetic model with multiple anisotropic structures involved. Finally, Section 6 discusses possible ways of extending the developed procedure to generally 3-D anisotropic structures.

2 Mathematical model of the problem

Let us assume a 2-D horizontally inhomogeneous and generally anisotropic model of the earth with a plane surface that separates the conductive earth from the air, which is considered a perfect insulator. The axes x and y of a Cartesian coordinate system identify the earth's surface, the vertical axis z points down into the earth. The electrical conductivity inside the earth is described by a symmetric, positive definite conductivity tensor $\boldsymbol{\sigma}(\mathbf{r})$, which can always be represented in terms of a diagonal matrix and three successive elementary Euler's rotations,

$$\boldsymbol{\sigma}(\mathbf{r}) \equiv \boldsymbol{\sigma}(y,z) = \mathbf{R}_z^T(\alpha_S)\mathbf{R}_x^T(\alpha_D)\mathbf{R}_z^T(\alpha_L) \begin{pmatrix} \sigma_1^P & 0 & 0 \\ 0 & \sigma_2^P & 0 \\ 0 & 0 & \sigma_3^P \end{pmatrix} \mathbf{R}_z(\alpha_L)\mathbf{R}_x(\alpha_D)\mathbf{R}_z(\alpha_S),$$

where σ_i^P, $i = 1,2,3$, are the principal conductivities, and $\mathbf{R}_a(\alpha)$ is the matrix of the elementary rotation around the current axis a by α. The superscript T is for the transposed matrix. If a simple dyke model of the anisotropic structure is considered, the directions α_S, α_D and α_L can easily be identified with the physically illustrative anisotropy strike, dip and slant, respectively (Fig. 1).

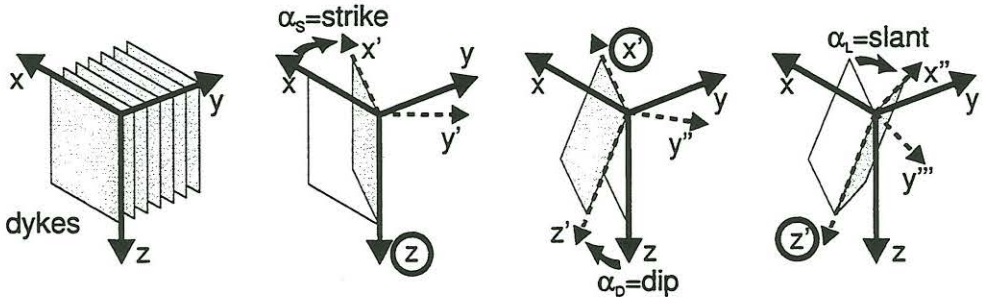

Figure 1: Simulation of the electrical anisotropy by means of a dyke model. The characteristic directions α_S (anisotropy strike), α_D (anisotropy dip) and α_L (anisotropy slant) are illustrated for one dyke. The rotation axis for each elementary rotation step is encircled.

The stationary electric field in the model is supposed to be generated by a system of N_Q point electrodes, which are situated at positions $\mathbf{r}_c$ inside the conductive halfspace or on its surface ($z_c \geq 0$) and feed the medium with the stationary currents I_c, $c = 1,2,\ldots,N_Q$. Then, the general equation for the current conservation law within the medium reads

$$\nabla \cdot \mathbf{J}(\mathbf{r}) = Q(\mathbf{r}), \tag{1}$$

with the source term in the form

$$Q(\mathbf{r}) = \sum_{c=1}^{N_Q} I_c \delta(\mathbf{r} - \mathbf{r}_c).$$

Assuming further a standard linear relationship between the current density and the intensity of the electric field, and employing the stationarity of the problem, which allows us to express the electric field in terms of a scalar potential,

$$\mathbf{J}(\mathbf{r}) = \boldsymbol{\sigma}(\mathbf{r})\mathbf{E}(\mathbf{r}), \quad \mathbf{E}(\mathbf{r}) = -\nabla\Phi(\mathbf{r}),$$

we finally can write (1) as

$$\nabla \cdot [\boldsymbol{\sigma}(\mathbf{r})\, \nabla\Phi(\mathbf{r})] = -Q(\mathbf{r}), \tag{2}$$

or, in the expanded form,

$$\frac{\partial}{\partial x}\left(\sigma_{xx}\frac{\partial\Phi}{\partial x} + \sigma_{xy}\frac{\partial\Phi}{\partial y} + \sigma_{xz}\frac{\partial\Phi}{\partial z}\right) + \frac{\partial}{\partial y}\left(\sigma_{yx}\frac{\partial\Phi}{\partial x} + \sigma_{yy}\frac{\partial\Phi}{\partial y} + \sigma_{yz}\frac{\partial\Phi}{\partial z}\right) +$$

$$+ \frac{\partial}{\partial z}\left(\sigma_{zx}\frac{\partial\Phi}{\partial x} + \sigma_{zy}\frac{\partial\Phi}{\partial y} + \sigma_{zz}\frac{\partial\Phi}{\partial z}\right) = -Q(x,y,z). \tag{3}$$

For a 2-D conductivity distribution, $\boldsymbol{\sigma} = \boldsymbol{\sigma}(y,z)$, the generally 3-D problem (3) can be substantially simplified by applying to (3) the Fourier transform with respect to the structural strike coordinate x, $\mathcal{F}_x f(x) = \int_{-\infty}^{\infty} f(x)\exp(-i\xi x)\,dx$. Then, the 3-D problem (3) gets decomposed into an infinite number of mutually independent 2-D problems in the ξ-wave-number domain with the following governing equations

$$\underbrace{\frac{\partial}{\partial y}\left(\sigma_{yy}\frac{\partial\phi}{\partial y}\right)+\frac{\partial}{\partial z}\left(\sigma_{zz}\frac{\partial\phi}{\partial z}\right)-\xi^2\sigma_{xx}\phi}_{\boxed{1}}+\underbrace{\frac{\partial}{\partial y}\left(\sigma_{yz}\frac{\partial\phi}{\partial z}\right)+\frac{\partial}{\partial z}\left(\sigma_{zy}\frac{\partial\phi}{\partial y}\right)}_{\boxed{2}}+$$

$$\underbrace{+i\xi\left(\sigma_{xy}\frac{\partial\phi}{\partial y}+\sigma_{xz}\frac{\partial\phi}{\partial z}\right)+i\xi\frac{\partial}{\partial y}(\sigma_{yx}\phi)+i\xi\frac{\partial}{\partial z}(\sigma_{zx}\phi)}_{\boxed{3}}=-q(\xi,y,z),\quad \xi\in(-\infty,\infty), \tag{4}$$

where $\phi(\xi,y,z)=\mathcal{F}_x\Phi(x,y,z)$ and $q(\xi,y,z)=\mathcal{F}_xQ(x,y,z)=\sum_{c=1}^{N_Q} I_c\delta(y-y_c)\delta(z-z_c)\exp(-ix_c\xi)$. The terms in eq. (4) have been rearranged to form three groups, which express specific aspects of the relation between the anisotropy and the potential. Except for different diffusion coefficients in the individual terms, the first part of (4), $\boxed{1}$, is identical with the corresponding equation for the isotropic case. The part $\boxed{2}$, with the conductivity elements σ_{yz} and $\sigma_{zy}(=\sigma_{yz})$, reflects the influence of the dipping anisotropy. In the simplified dyke model, the terms of $\boxed{2}$ arise due to oblique dykes that run, however, parallel to the structural strike of the model. If the anisotropy strike differs from that of the 2-D model, terms in $\boxed{3}$ appear, which are always complex, and cause the wave number components of the potential, $\phi(\xi,y,z)$, to be complex for $\xi\neq 0$ in generally anisotropic media.

The infinite set of 2-D PDEs (4) represents the basis of the mathematical model of our problem. For its solution, the conditions for the potential components $\phi(\xi,y,z)$ on both the internal and external boundaries of the model must be further provided. These conditions are of general character, and require, for any wave number $\xi\in(-\infty,\infty)$, the potentials $\phi(\xi,y,z)$ and the normal current densities, $j_n(\xi,y,z)=-\mathbf{n}\cdot\boldsymbol{\sigma}(y,z)\nabla_2\phi(\xi,y,z)$, to be continuous at any internal boundary, $\mathbf{n}$ being the unit normal vector to the boundary, and $\nabla_2=(i\xi,\partial/\partial y,\partial/\partial z)$. The latter condition also applies to the normal currents on the earth's surface, where it reduces to $j_z=-i\xi\sigma_{zx}\phi-\sigma_{zy}\partial\phi/\partial y-\sigma_{zz}\partial\phi/\partial z=0$, due to the zero conductivity of the air. The conductivities of the medium from immediately below the earth's surface, i.e. at $(y,z\to 0+)$, are considered in this condition. Exceptions to this condition are singular points through which the currents are injected into the model, i.e. points at which the feeding point electrodes are situated.

There is more freedom in choosing the external boundary conditions at $y\to\pm\infty$ and $z\to+\infty$. In our model formulation, we impose the simple Dirichlet condition, $\phi=0$, at those external boundaries.

3 FD approximation of the problem, numerical solution

3.1 Approximation by the area discretization (volume integration)

To solve the problem (4) numerically, we use the FD technique in essentially the same way as it was used for solving the 2-D problem for isotropic structures by Dey & Morrison [1]. At first, the model is overlaid with an non-regular orthogonal FD mesh, consisting of (N_y+1) vertical mesh lines $y=y_j$, $j=0,1,\ldots,N_y$, and (N_z+1) horizontal mesh lines $z=z_k$, $k=0,1,\ldots,N_z$. The mesh divides the model domain into a system of rectangular mesh cells G_{jk}, $j=1,2,\ldots,N_y$, $k=1,2,\ldots,N_z$, with the widths $h_j^{(y)}=y_j-y_{j-1}$, $j>0$, and heights $h_k^{(z)}=z_k-z_{k-1}$, $k>0$. For simplicity, we assume that the mesh cells are homogeneous, with a local conductivity tensor $\boldsymbol{\sigma}_{jk}$, and that the internal model boundaries coincide with sections of the mesh lines.

The top horizontal mesh line, $z=z_0=0$, coincides with the earth's surface. The marginal mesh lines, $y=y_0$, $y=y_{N_y}$ and $z=z_{N_z}$, are supposed to be situated far enough from the 2-D inhomogeneities, as well as from the current sources, to allow us to apply the Dirichlet conditions $\phi=0$ on the outer boundaries of the finite model domain, except the earth's surface where the vertical current density must vanish.

In order to FD approximate the PDEs (4) in the vicinity of an arbitrary mesh node, we have adopted the 'area discretization scheme' of Dey & Morrison [1], more commonly known as a volume integration

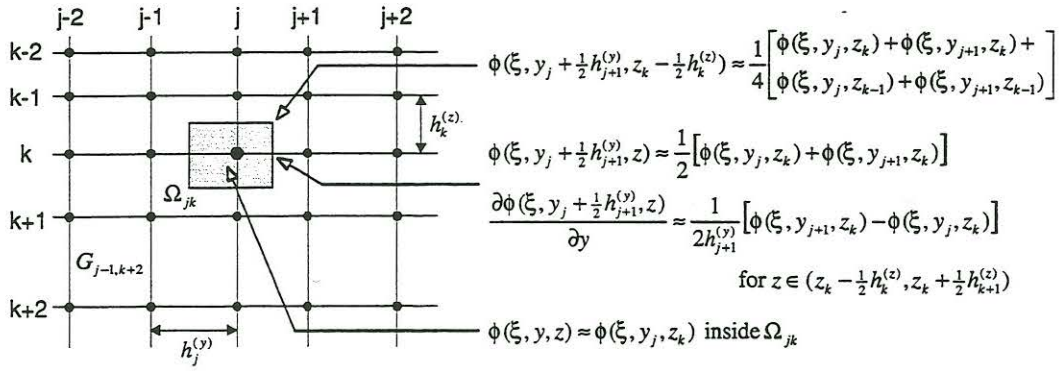

Figure 2: A section of the FD mesh in the vicinity of the (j,k)-th mesh node, and the integration cell Ω_{jk}. For relevant points, the formulae used in the course of the approximate evaluation of integral (5) are shown.

approach. Principally, this scheme, instead of treating directly the differential equations (4), approximates the integral form of the current conservation law in a close vicinity of the mesh node involved. Across a local rectangular integration cell, specifically $\Omega_{jk} = (y_j - \frac{1}{2}h_j^{(y)}, y_j + \frac{1}{2}h_{j+1}^{(y)}) \times (z_k - \frac{1}{2}h_k^{(z)}, z_k + \frac{1}{2}h_{k+1}^{(z)})$ for the (j,k)-th node (see Fig. 2), we suppose

$$\int_{\Omega_{jk}} \{\nabla_2 \cdot [\sigma(y,z)\nabla_2\phi(\xi,y,z)] + q(\xi,y,z)\}\, dy\, dz = 0, \qquad \xi \in (-\infty, \infty), \tag{5}$$

where the integrand of (5) is a more compactly written, but equivalent form of (4).

Although tedious, the algebra involved in the evaluation of the above integrals is rather straightforward. The individual terms of (5) are integrated separately across the homogeneous sub-rectangles of the integration cell Ω_{jk}, and connected via the general boundary conditions on the internal interfaces. For the mesh nodes located on the earth's surface, the integration is carried out across the lower half of the integration cell only, and the boundary condition $j_z(\xi, y, z \to 0+) = 0$ is made use of. At marginal nodes of the model domain, the respective boundary conditions are substituted for the potential values along the outer boundaries. In Fig. 2, the basic formulae are listed used to approximate the potential and its spatial derivatives at specific points of the integration cell.

Without going into detail of the individual evaluation steps, we will present only the results of the approximation procedure here. Evaluating the integral (5), and carrying out the approximations as shown schematically in Fig. 2, leads eventually, at each internal or surface mesh node $(j,k) \in \{1, 2, \ldots, N_y - 1\} \times \{0, 1, \ldots, N_z - 1\}$, to one FD linear algebraic equation, which relates, in general, the potential at the central node to all its eight neighbours in the mesh. The resulting 9-point FD stencil is shown in Fig. 3. Comparing this stencil with that for the isotropic problem, the main differences can be summarized as follows:

a) The positions of the diagonal neighbours of the central node are occupied by coefficients that depend on σ_{yz} only, i.e. these coefficients result from the dipping anisotropy (terms $\boxed{2}$ in eq. (4)). They also contribute to the central node coefficient through $\lambda_{yz}(j,k)$.

b) The effect of the anisotropy strike and slant (or, more exactly, of the conductivity elements σ_{xy} and σ_{xz}, terms $\boxed{3}$ in eq. (4)) is expressed by modified coefficients for the direct neighbours of the central node. Due to the anisotropy, these coefficients are in general complex. Due to the symmetry of the conductivity tensor, the conductivity elements σ_{xy} and σ_{xz} do not directly affect the central node coefficient.

c) In the isotropic case, the evident relations $R_{jk} = Q_{j,k+1}$ and $S_{jk} = P_{j+1,k}$ guaranteed the symmetry of the matrix of the linear FD equations (with proper ordering of the nodes throughout the mesh assumed). For anisotropic models, only the real parts of the coefficients within the FD stencil meet the above symmetry conditions. The imaginary parts are, however, antisymmetric, so that the above relations change to

$$R_{jk} + 2i\xi R_{jk}^{(xz)} = (Q_{j,k+1} - 2i\xi Q_{j,k+1}^{(xz)})^*, \qquad S_{jk} + 2i\xi S_{jk}^{(xy)} = (P_{j+1,k} - 2i\xi P_{j+1,k}^{(xy)})^*, \tag{6}$$

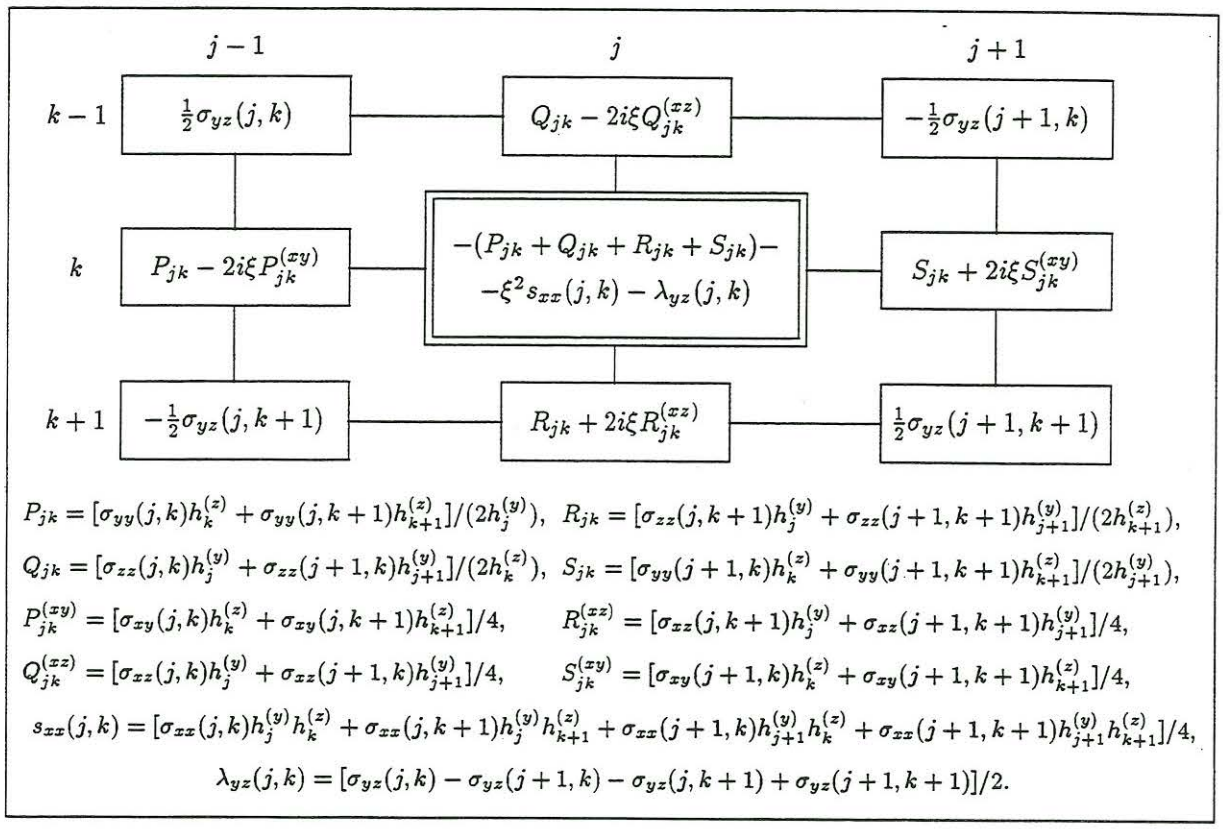

Figure 3: 9-point stencil for the node (j, k), resulting from the FD approximation of eq. (4).

where the asterisk means complex conjugation. With (6), the system of FD equations is complex, non-symmetric, but Hermitian, if the nodes are ordered properly.

Integrating the source term in (5), we obtain

$$\int_{\Omega_{jk}} q(\xi, y, z)\, dy\, dz = \begin{cases} I_{c_E} \exp(-i x_{c_E} \xi), & \text{if } (y_{c_E}, z_{c_E}) \in \Omega_{jk}, \\ 0, & \text{if no electrode is located inside } \Omega_{jk}. \end{cases}$$

With a known configuration of the current electrodes, the above source term approximations are completely known, and contribute to the right-hand side of the FD equation system only. Moreover, considering the superposition principle, a multiple-source solution can always be obtained as a sum of correspoding single-source solutions. Then, with one feeding electrode only, the coordinate system can be always shifted along the strike of the 2-D model to have $x_{c_E} = 0$, avoiding thus the inconvenience of a complex right-hand side of the FD system.

3.2 Structure and solution of the FD equation system

The complete set of the linear FD equations, obtained at the individual mesh nodes, is further arranged into a system of linear algebraic equations for the approximate potentials $\phi(\xi, y_j, z_k)$. The form of the matrix of this system depends on in which way the nodes are ordered throughout the mesh. For the traditional column-wise ordering, the indices of internal and surface mesh nodes are mapped onto a one-dimensional array of ordinal numbers by

$$\boxed{\{(j,k) \,|\, j = 1, \ldots, N_y - 1, z = 0, \ldots, N_z - 1\}} \rightarrow \boxed{\{\ell \,|\, \ell = (j-1)N_z + k + 1, \ell = 1, \ldots, (N_y - 1)N_z\}}.$$

With this arrangement of the mesh nodes, the matrix of the FD linear system is a 9-diagonal, sparse and banded matrix, with the band width $2N_z + 3$. In general, it is complex, non-symmetric, but Hermitian.

For the solution of the above linear system of the FD equations, the well known algorithm of the Gaussian elimination for symmetric banded matrices, slightly modified to deal with Hermitian matrices,

can be used, if the numerical problem is of reasonable size, of course. The advantage of solving systems with multiple right-hand sides (e.g., for multiple feeding electrodes, or for parameter sensitivities) at substantially reduced costs is preserved in the modified elimination algorithm. Moreover, in the initial stage of the algorithm design, it is advantageous to use a direct method for the solution of the large FD linear system, as difficulties with distinguishing the deficiencies of the numerical solution resulting from a defect approximation scheme on the one hand from those originated in poor properties of an iterative solver on the other can be avoided.

3.3 Fourier synthesis of the potential

Due to the complexity of the FD matrix in the anisotropic case, the resulting potential components $\phi(\xi, y_j, z_k)$ will be complex as well, except for $\xi = 0$. In virtue of the special Hermitian symmetry of the FD matrix, induced by the antisymmetry of the imaginary wave-number-dependent terms in the FD stencil in Fig. 3, the potential componets conform the condition $\phi(-\xi, y_j, z_k) = \phi^*(\xi, y_j, z_k)$ for any ξ. Thus, the resulting total potential $\Phi(x, y_j, z_k)$, given by the Fourier synthesis,

$$\Phi(x, y_j, z_k) = \mathcal{F}_\xi^{-1}\phi(\xi, y_j, z_k) = \frac{1}{2\pi}\int_{-\infty}^{\infty} \phi(\xi, y_j, z_k)\exp(+ix\xi)\,d\xi =$$

$$= \frac{1}{\pi}\int_0^{\infty} \{\Re[\phi(\xi, y_j, z_k)]\cos x\xi - \Im[\phi(\xi, y_j, z_k)]\sin x\xi\}\,d\xi, \tag{7}$$

is a real function, as required by the problem's physics.

For different wave numbers ξ, different FD approximate equations are obtained by the approximation described in section 3.1. The wave number ξ enters into the coefficients of the central node and of its direct neighbours in the FD stencil (Fig. 3), and, consequently, into both the diagonal and non-diagonal elements of the FD matrix. For each individual wave number ξ, one system of the FD equations must be solved in full, which makes the total costs of the problem solution to be highly dependent on the selection of the particular wave number spectrum used for the potential approximation. For isotropic 2-D modelling algorithms, very economical sets of cautiously selected wave numbers have been suggested to approximate the total potential with high accuracy by not more than ten wave number components [1]. That possibility is given by the real and monotonous character of the wave number potential components $\phi(\xi, y, z)$ as functions of ξ in the isotropic case. With a coarse wave number spectrum, Dey & Morrison [1] could achieve high accuracy results by piece-wise approximating the wave number potential $\phi(\xi, y, z)$ by exponentials, and, subsequently, by integrating the isotropic analogue of (7) analytically.

Unfortunately, the above mentioned properties of the potential are no more valid for models with anisotropy. The Fourier synthesis for this case is expressed by formula (7), with $\Im[\phi(\xi, y, z)] \neq 0$ in general. Moreover, neither $\Re[\phi(\xi, y, z)]$ nor $\Im[\phi(\xi, y, z)]$ are monotonous functions of ξ. Already for the simple case of a homogeneous anisotropic halfspace with a general anisotropy strike α_S and with resistivities ϱ_L along and ϱ_T transversaly to the anisotropy strike, both the real and imaginary parts of $\phi(\xi, y, z)$ oscillate along the ξ-axis. The origin of the oscillations can be easily seen from the analytical formula for the simple model considered [5],

$$\phi(\xi, y, z) = \frac{I\sqrt{(\varrho_L\varrho_T)}}{\pi\gamma}\,\mathrm{K}_0\left(\frac{\sqrt{(\lambda^2 y^2 + \gamma^2 z^2)}}{\gamma^2}\xi\right)\exp\left(iy\,\frac{(1-\lambda^2)\sin\alpha_S\cos\alpha_S}{\gamma^2}\xi\right),$$

where $\lambda^2 = \varrho_T/\varrho_L$ (with $\varrho_L < \varrho_T$ assumed), $\gamma^2 = \cos^2\alpha_S + \lambda^2\sin^2\alpha_S$, and K_0 is the modified Bessel function of the order zero. The current electrode is supposed to be located at $\mathbf{r}_E = (0, 0, 0)$. The oscillations result from the exponential term in the above formula, and are modulated by the rapidly decreasing, but positive K_0-term. The frequency of the oscillations depends on the distance from the source electrode y, as well as on the anisotropy parameters. The oscillatory character of $\phi(\xi, y, z)$ disappears for $\lambda = 1$ (isotropic case) and for $\alpha_S = 0°$ or $90°$ (strike-parallel or strike-perpendicular anisotropy, respectively).

For 2-D models with general anisotropy, the frequency of the oscillations is unpredictable, so that it is hardly possible to suggest one simple set of wave numbers, which would represent the total potential with sufficient accuracy in the wave number domain. Moreover, the oscillatory character of $\phi(\xi, y, z)$, with unknown frequency, must be considered in any attempt to locally approximate the potential by analytical functions. We admit that we have not solved this problem satisfactorily as yet, and have applied a rather brute force approach, by selecting an excessively large set of 30 to 50 densely log-regularly distributed

wave numbers to approximate the potential and compute the integral (7) by the simple trapezoidal integration rule. This approach increases the computation costs of the algorithm considerably. Further experiments are being carried out at present to find a more convenient and cheaper representation of the potential in the wave number domain.

4 Numerical tests of the algorithm

So far, only basic tests of the algorithm for the 2-D modelling of direct currents in anisotropic structures have been performed. The only 2-D model for which an analytical solution is available is that of the homogeneous anisotropic halfspace [5]. Recently, quasi-analytical solutions have been presented for two more model types, specifically a two-layer anisotropic medium [6] and vertical contacts in an anisotropic halfspace [7][1], which we intend to use for further testing.

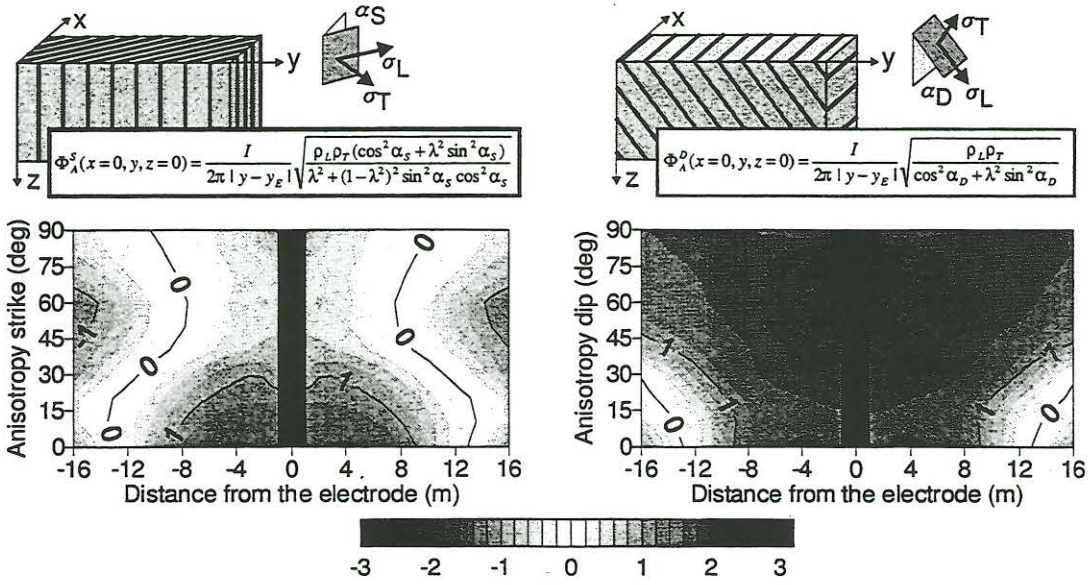

Figure 4: Comparison of the pole-pole apparent resistivities predicted from the potentials computed numerically with those obtained from known analytical formulae for the model of a homogeneous anisotropic halfspace. The gray-shade plots show the difference between the numerical and the corresponding analytical values in per cent. Left-hand panel—The anisotropy strike differs from the structural strike, $\alpha_S \in \langle 0°, 90° \rangle$. In the top panel, the model is schematically shown by a dyke scheme, and the corresponding analytical formula from [5] is given as well. Right-hand panel—Analogous comparison of the numerical and analytical results for a model with dipping anisotropy, $\alpha_D \in \langle 0°, 90° \rangle$.

In Fig. 4, we test the accuracy of the potential computations performed by our numerical procedure by comparing our results with the corresponding values computed analytically for two simple models of the anisotropic halfspace, one with different strikes of the anisotropy and the structure, and the other with dipping anisotropy. The computations were performed for a single current electrode in the center of the model. The FD mesh was designed quasi-homogeneously (i.e. with mostly regular horizontal steps, but with slightly higher mesh line density in the immediate vicinity of the feeding electrode) across the area of the model shown in the figure. Further towards the vertical boundaries of the model, as well as down into the earth, the mesh steps increased progressively with the factor of 1.2. Fourty five wave numbers were used to represent the potential, distributed log-regularly within the interval 10^{-3} to about 50 m^{-1}. The obtained results show a good coincidence of the pole-pole apparent resistivities recovered from the numerically calculated potential and those obtained analytically. The differences do not exceed 3 per cent for any parameter combination within the displayed area.

[1]The authors wish to express their thanks to Dr. Klaus Spitzer, BGR Hannover, for providing them with the reference to P. Li's and N. F. Uren's latest publications on the DC anisotropy subject.

5 Examples of 2-D numerical simulations

As the algorithm is still in the phase of development, we have not so far used any experimental data to demonstrate its performance. We have computed several schematic models to get an idea about possible effects of anisotropic structures on DC data. As an example, we present here a model example, which we earlier studied, on a larger scale, by our 2-D modelling algorithm for magnetotelluric fields [3]. The model consists of a buried anisotropic layer and an outcropping anisotropic block, which rests on top of the layer. The anisotropies of the two bodies are, in general, different, both as to the principal conductivities and the anisotropy directions.

Fig. 5 shows the apparent resistivity contours for three variants of this model. The apparent resistivities are computed for a multi-electrode measurement configuration, with an array of 33 equidistantly positioned electrodes, spacing 1 m. The electrodes are used alternately as feeding and potential electrodes, and produce apparent resistivities corresponding to a combined Schlumberger and Wenner profiling. The distance between the current electrodes varies so as to cover 12 depth levels.

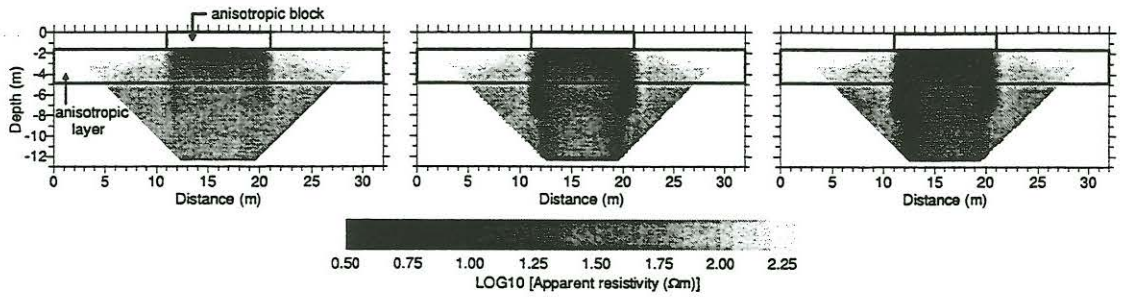

Figure 5: Apparent resistivity contours for a model of an anisotropic layer with an outcropping anisotropic block on top of it. The layer is at the depth of 1.65 m, and is 3.2 m thick. The outcrop is 10 m wide and is situated between the surface and the top boundary of the layer. The position of the anisotropic bodies is indicated by bold rectangles in all the plots. The resistivity of the host medium is 300 Ωm. In the left-hand panel, both bodies are only horizontally anisotropic, with the the same electrical parameters: longitudinal resistivity $\varrho_L = 10$ Ωm, transversal resistivity $\varrho_T = 100$ Ωm, and anisotropy strike $\alpha_S = 45°$ with respect to the structural strike of the model. In the central panel, the block is the same as above, but the anisotropy strike of the underlying layer changed to $\alpha_S^{\text{layer}} = 135°$, i.e. the directions of the preferred conductivity in the block and in the layer are perpendicular to one another. In the right-hand panel, anisotropy dip is introduced into the previous model. The anisotropy directions are: $\alpha_S^{\text{block}} = 45°$, $\alpha_S^{\text{layer}} = 135°$, and $\alpha_D^{\text{block}} = \alpha_D^{\text{layer}} = 30°$.

For simplicity, we assume the anisotropic resistivity of both the bodies involved to be defined via two different principal resistivities only—ϱ_L parallel to the anisotropy strike, and ϱ_T in the perpendicular direction. Moreover, we set $\varrho_L = 10$ Ωm and $\varrho_T = 100$ Ωm in both structures. The anisotropic block, 10 m wide and 1.65 m thick, is just at the lower limit of the depth resolution of the simulated measurement configuration. The underlying anisotropic layer, 3.20 m thick, is expected to dominate most of the upper part of the resistivity pseudosection.

In the left panel of Fig. 5, both the layer and the block are only horizontally anisotropic, both with the identical anisotropy strike $\alpha_S = 45°$ with respect to the structural strike of the model. The outcropping block affects the central part of the pseudosection by decreasing the resistivities to about 13.5 Ωm, the value for the anisotropic halfspace with the same electrical parameters, at the top of the section. The effect of the outcrop diminishes with depth, and the pseudosection gets homogenized, with resistivities of 50 to 60 Ωm.

The central panel of Fig. 5 shows a similar situation as the previous example, only the anisotropy strike of the anisotropic layer is changed to $\alpha_S^{\text{layer}} = 135°$. Thus, the anisotropy strike of the block and that of the underlying layer are perpendicular to one another. This model produces anomalous apparent resistivities, in particular near the edges of the anisotropic block, where narrow side lobes with anomalously low resistivities appear, as low as 6 Ωm at the centers of the lobes. This anomalous effect is further amplified if the plane of the preferred conductivity of the anisotropic structures is deflected from the vertical. Results in the right-hand panel of Fig. 5 were obtained for the previous model with the

anisotropy dip $\alpha_D = 30°$ additionaly applied to the conductivity tensor of each of the anisotropic domains. As a result, the pseudosection becomes non-symmetric, with the low resistivity side lobe developed more intensely below the left edge of the block (minimum resistivity of about 1.6 Ωm), and reduced below the oposite edge (to about 12 Ωm at the center).

Though highly artificial, the above modelling example shows that the anisotropy within the geoelectrical section can cause serious distortions of the DC potentials on the surface. More practice-oriented model simulations are, however, required to make more qualified conclusions as to the real influence of anisotropic structures on DC measurements.

6 3-D perspectives of the problem

It is logical to finish the description of the algorithm by giving an idea about its possible extensions, especially to the 3-D media. A generalization of the 2-D numerical modelling procedure, described in the previous text, to 3-D models does not, in principle, represent any serious problem. As there is no qualitative change in the formulation of the problem when passing from two to three dimensions, the theoretical and approximation phase of the 3-D problem seems to be even simpler than that of the 2-D case, as the certain 'anisotropy', introduced by the exclusiveness of the strike coordinate in 2-D, disappears. We can present here a few preliminary results of the approximation phase for the 3-D problem, which can be a good starting point for a numerical realization of the 3-D modelling algorithm in the future.

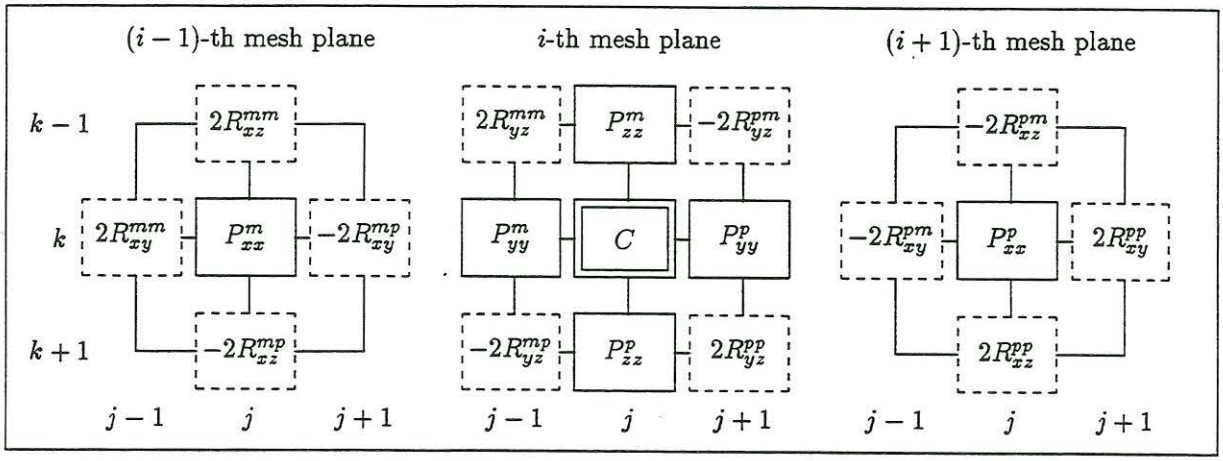

Figure 6: Slices, along the x-axis, of the 19-point FD stencil resulting from the FD approximation of the 3-D PDE (3) at the (i, j, k)-th mesh node. The central node is provided with a double frame, its direct neighbours are single framed, and its near-diagonal neighbours, arising due to anisotropy, are marked by dashed frames. The far-diagonal positions, like, e.g., $(i+1, j-1, k+1)$, are unoccupied in this discretization scheme.

Applying the volume integration approach in the very same way as we did in the 2-D case, we can quickly arrive at the FD approximation scheme for the general 3-D equation (3). The resulting 19-point FD stencil for the (i, j, k)-th mesh node is shown in Fig. 6 in the form of three successive slices along the x-coordinate axis. A general cyclic rule can be deduced according to which the coefficients in this stencil can be easily constructed, and, e.g.,

$$P^p_{yy} = [\sigma_{yy}(i, j+1, k)h_i^{(x)}h_k^{(z)} + \sigma_{yy}(i+1, j+1, k)h_{i+1}^{(x)}h_k^{(z)} + \sigma_{yy}(i, j+1, k+1)h_i^{(x)}h_{k+1}^{(z)} + \\ + \sigma_{yy}(i+1, j+1, k+1)h_{i+1}^{(x)}h_{k+1}^{(z)}]/(4h_{j+1}^{(y)}),$$

$$R^{pm}_{xy} = [\sigma_{xy}(i+1, j, k)h_k^{(z)} + \sigma_{xy}(i+1, j, k+1)h_{k+1}^{(z)}]/8,$$

and

$$C = -(P^m_{xx} + P^p_{xx} + P^m_{yy} + P^p_{yy} + P^m_{zz} + P^p_{zz}) - 2(R^{mm}_{xy} - R^{pm}_{xy} - R^{mp}_{xy} + R^{pp}_{xy}) - \\ -2(R^{mm}_{xz} - R^{pm}_{xz} - R^{mp}_{xz} + R^{pp}_{xz}) - 2(R^{mm}_{yz} - R^{pm}_{yz} - R^{mp}_{yz} + R^{pp}_{yz}).$$

Using the column-wise ordering of the mesh nodes throughout the mesh, the approximation of the 3-D problem results in a large system of linear FD equations, with a 19-diagonal, sparse and banded, symmetric real matrix. The size of the matrix is $(N_x - 1)(N_y - 1)N_z$, and its bandwidth $2N_yN_z + 1$. Even for moderate-size problems, the linear system is very large, and iteration solvers must be used to find its solution. Spitzer & Wurmstich [8] made a thorough comparison of various CG-like solvers with preconditioning for the 3-D FD modelling in isotropic structures. The anisotropy, in general, increases the condition number of the normal FD matrix [9], making the linear system more difficult to solve. A thorough selection of suitable preconditioners and coefficient adaptive mesh transformations have been recommended to improve the numerical properties of the iterative solvers for large anisotropic problems [9].

7 Conclusion

In this paper, a basic form of an algorithm for the 2-D modelling of direct currents in anisotropic structures has been presented. The volume integration version of the FD method was used to numerically approximate the problem. As compared to the isotropic case, two differences are worth mentioning for anisotropic models. First, the problem leads to a 9-point FD stencil, with diagonal neighbours of the central node involved, and, second, the normal FD matrix for the wave number potential components is complex and non-symmetric, but Hermitian. With this type of symmetry, the procedure for solving the anisotropic problem does not differ substantially from that used in the isotropic case.

The procedure presented here is still a preliminary version of the algorithm. Several important steps are still to be done, in particular (i) improving estimates of the accuracy of the algorithm, and testing it on 2-D analytical data for more complex models with anisotropy, (ii) optimizing the inverse Fourier transform of the wave number potential components, and (iii) testing more accurate asymptotic conditions, with the aim to reduce the mesh size for the problem.

References

[1] Dey, A. & Morrison, F., 1976: Resistivity modeling for arbitrarily shaped two dimensional structures, Part I: Theoretical formulation, *Report LBL-5223*, Lawrence Berkeley Laboratory, Univ. of California/Berkeley, pp. 1–18.

[2] Karous, M.: *Geoelectrical prospecting methods*, SNTL/Alpha, Prague 1989, pp. 1–424 (in Czech).

[3] Pek, J. & Verner, T., 1997: Finite-difference modelling of magnetotelluric fields in two-dimensional anisotropic media, *Geophys. J. Int.*, **128**, 505–521.

[4] Weidelt, P., 1996: Elektromagnetische Induktion in dreidimensional anisotropen Leitern, in *Protokoll Kolloquium 'Elektromagnetische Tiefenforschung', Burg Ludwigstein 9.–12. 4. 1996*, eds. Bahr, K. and Junge, A., DGG, pp. 60–73.

[5] Yakubovski, Yu. V.: *Electrical prospecting*, Nedra Publishing, Moscow 1973, pp. 1–302 (in Russian).

[6] Li, P. & Uren, N. F., 1997: Analytical solution for the point source potential in an anisotropic 3-D half-space I: Two-horizontal-layer case, *Mathem. Comp. Modelling*, **26**, 9–27.

[7] Li, P. & Uren, N. F., 1997: Analytical solution for the point source potential in an anisotropic 3-D half-space II: With two-vertical boundary, *Mathem. Comp. Modelling*, **26**, 29–52.

[8] Spitzer, K. & Wurmstich, B., 1996: Speed and accuracy in 3-D resistivity modeling, in *Protokoll Kolloquium 'Elektromagnetische Tiefenforschung', Burg Ludwigstein 9.–12. 4. 1996*, eds. Bahr, K. and Junge, A., DGG, pp. 228–240.

[9] D'Azevedo, E. F., Romine, C. H. & Donato, J. M., 1995: Coefficient adaptive triangulation for strongly anisotropic problem, *Report ORNL/TM-13086*, Oak Ridge National Laboratory, pp. 1–13.